Intimate Control for UAV and UGV Rendezvous and Docking: Refined Analysis and Robustness

Tony Griffiths
MBDA UK Ltd, PO Box 5, Filton, BS34 7QW

Abstract

CC010 considers control strategies for dealing with systems in close proximity that are involved in docking while manoeuvring. Such control strategies form a new area of control engineering called intimate control. This short paper summarises the Phase 2-Stage 2 Refined Analysis report [0] which examines the robustness of this intimate control algorithm when the dynamics and error characteristics of the proposed sensors and communications [0] are taken into account. This rendezvous study also takes into account the effects of road roughness and wind turbulence, including shear and gusting for wind speeds of up to 15m/s, and gust amplitudes of between 3-3.5m/s.

Keywords : Collaborative Control, Intimate Control, Docking, Rendezvous, UAV, UGV, GPS, Terrain Roughness, Turbulence, Shear, Gusting

Introduction

For manned in-flight refuelling tasks, the full capabilities of the two docking agents are frequently underutilised. Automation via Intimate Control [0] was introduced to allow the agents to exploit their respective capabilities to the full to meet the docking constraints. As a practical first step towards demonstrating the refuelling capability, a ground based demonstration between a UGV and a UAV would be able to represent the essential features of the Intimate Control solution.

This SEAS DTC rendezvous project was sub-divided into three phases of development: Phase 1, Analysis of potential vehicles and algorithms [0]; Phase 2, Feasibility study of rendezvous over a series of mission phases through 6DOF modelling [0,0]; Phase 3, full hardware and software demonstration.

This collaborative control solution consists of two distinct control phases. The first phase is the independent control of the UAV, using a rendezvous guidance algorithm (RG) to manoeuvre the UAV to within the acquisition range of the laser tracker. Then having accomplished this rendezvous manoeuvre a second control phase, the 'intimate control' (IC) phase is entered to achieve the final docking.

The Collaborative Control Simulation (CCS) 6DOF model reported in [0] was used to investigate the robustness of the proposed intimate control scheme using the sensors and communications characteristics reported in [0]. The chosen rendezvous vehicles used in this robustness study, are the XRAE UAV [0], with a speed of operation in the range ~20-30m/s, and the BAE Systems ATC Wildcat with a top speed of 36m/s [0].

Terrain Roughness and UGV Suspension

The UGV suspension transfer function model used in [0] was replaced by the SIMULINK simplified half-car model. This suspension model was modified to include the docking torque, resulting from the UAV making contact with the UGV, together with the road roughness disturbance, acting through the suspension. A comparison of the output from this suspension model with

the data obtained from [0] shows reasonable agreement, see Figure 1.

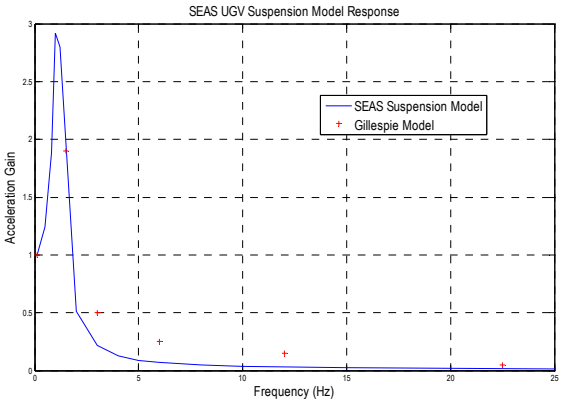

Figure 1: Simulated Passive Suspension

Table 1: ISO Road Roughness Data

Classification $S(\Omega)$	Road Roughness $\kappa[m^2/(cycles/m)]$
A (Very Good)	4e-6
B (Good)	16e-6
C (Average)	64e-6
D (Poor)	256e-6
E (Very Poor)	1024e-6

The ISO road roughness characterisation in [0] was modelled in the CCS 6DOF, see Table. This roughness characterisation produced road displacements ranging from $0.2\text{m}(3\sigma)$ to $3.4\text{m}(3\sigma)$, for motorways and very rough roads respectively, for a simulated 4km road segment, as shown in Figure 2.

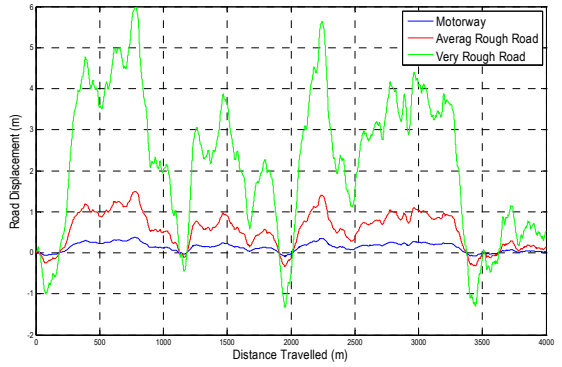

Figure 2: SEAS Modelled Road Roughness

Inclusion of Air Brake, Actuator, and IMU, GPS, and Laser Tracker Models

To avoid appreciable speed build up during descent [0] the CCS model was modified to allow the XRAE UAV to deploy an air brake during descent. The air brake was simulated by increasing the drag coefficient by 50% using:

$$C_D = 1.5\left(C_{D0} + \left(\frac{\partial C_D}{\partial C_L^2}\right)C_L^2\right)$$

where C_{D0} is the base drag, and $\left(\frac{\partial C_D}{\partial C_L^2}\right)C_L^2$ is the lift induced drag.

The actuator was modelled using the following second order representation:

$$Act(s) = \frac{\omega_{act}^2}{\left(s^2 + 2\varsigma_{act}\omega_{act}s + \omega_{act}^2\right)},$$
$$\omega_{act} = 2\pi 15, \quad \varsigma_{act} = 1/\sqrt{2}$$

where the 15Hz bandwidth has been taken from [0]. The modelled actuator non-linearities include the 6.5rad/s rate limit, together with the following position limits:

$$|\xi|_{\max} = 18^\circ, |\eta|_{\max} = 14^\circ, |\varsigma|_{\max} = 13.6^\circ$$

for the aileron, elevator and rudder respectively.

The IMU model was produced using the second order characteristic:

$$Gyro(s) = Accel(s) = \frac{\omega^2}{\left(s^2 + 2\varsigma\ \omega\ s + \omega^2\right)},$$
$$\omega\ = 2\pi 80, \quad \varsigma = 1/\sqrt{2}$$

together with the error characteristics shown in Table 2.

Using these actuator characteristics the XRAE test harness described in [1] was used to examine the response of the airframe to a series of height, speed and yaw commands as shown in Figure 3. Initially in these plots, the speed is commanded to reduce to approximately

24m/s to maximise the induced drag during descent. (This minimum descent speed must be chosen to avoid the stall region just below 20m/s). Then having descended to an altitude of 10m, the vehicle is commanded to increase its yaw angle by 20 deg. In addition to achieving their requested step response values, see Figure 3, the plots of pitch angle θ, and angle of attack α also exhibit an oscillatory component.

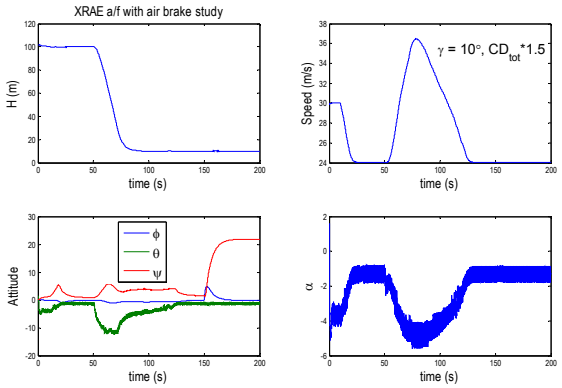

Figure 3: XRAE Response including Actuator and Air Brake

As an interim solution to this oscillation and to prevent the fins from limiting, the control and adaption gains in the XRAE non-linear adaptive autopilots were initially modified to improve stability. The resulting improved test harness results for the modified autopilots are shown in Figure 4, and repeated in Figure 5 for a 5m/s wind speed case.

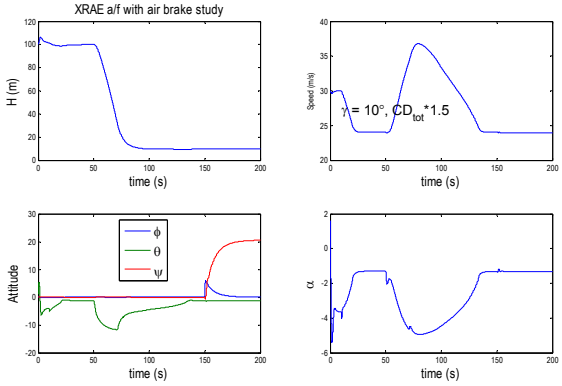

Figure 4: Modified XRAE Autopilot, including Actuator and Air Brake

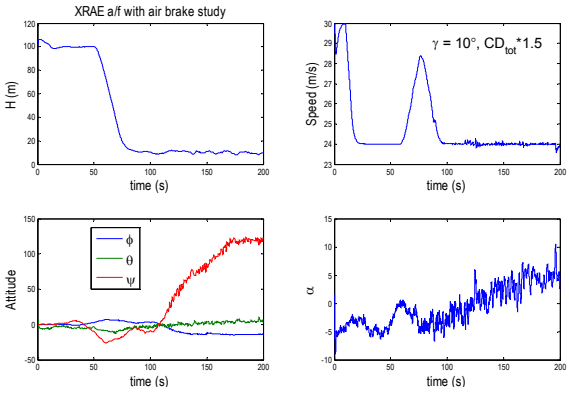

Figure 5: Modified XRAE Autopilot, including Actuator, Air Brake, and Wind Disturbance (5m/s)

Table 2: IMU Errors

	Gyro	Accelerometer
Range	$>\pm 500^\circ/s$	$\pm 30g$
Bias	$<0.13^\circ/s$	$<17mg$
Scale Factor	$<0.025\%^*$	$<0.1\%^*$
Random Walk	$1^\circ/\sqrt{hr}^*$	$<1ms^{-1}/\sqrt{hr}^*$
Bandwidth	$80Hz$	$80Hz$
Mis-alignment	1.7mrad	1.7mrad
Noise	$1.5^\circ/s$	$20mg$

The Laser tracking position and angle errors used in the CCS model, taken from the requirement in [2] are:

$$\Delta R = 0.1\ m$$

$$\Delta\theta = \frac{2\pi}{180}\ rad$$

To improve the accuracy in the vertical direction it is assumed that a radar altimeter, with an accuracy of 1m (ΔH_{ra}), is used for altitudes above 6m. For altitudes less than 6m an ultrasonic altimeter, with an accuracy of 0.025m (ΔH_{us}), is used for the final approach and docking.

The North $\Delta P_{\text{north,}}$ and East ΔP_{east} position measurement errors are scheduled with range $\|P_{\text{ag}}\|_2$ using:

$$\Delta P^{\text{lga}}_{North,East} = \begin{cases} \Delta P_{\text{GPS}} \; if \; \|P_{\text{ag}}\|_2 \geq 50 \; m \\ \Delta P_{\text{laser}} \; if \; 6 \leq \|P_{\text{ag}}\|_2 < 50 \; m \end{cases}$$

and for the Down errors, using:

$$\Delta P^{\text{lga}}_{Down} = \begin{cases} \Delta H_{\text{ra}} \; if \; \|P_{\text{Down}}\|_2 \geq 6 \; m \\ \Delta H_{\text{us}} \; if \; \|P_{\text{Down}}\|_2 < 6 \; m \end{cases}$$

where the GPS errors ΔP_{GPS} are shown in Table 3:

GPS Position Errors (ΔP_{GPS})	Bias (m)	Random (m)
Horizontal 1σ	7.7381	3.5173
Vertical 1σ	13.5069	6.1395

Table 3: GPS Errors

Performance and Robustness to Wind Disturbance

Wind Turbulence is modelled using the SIMULINK block which is based on the mathematical representation as defined in the Military Specification MIL-F-8785C [0]. Using this MIL-F-8785C wind specification, turbulence scale factor lengths of 300m were chosen to correspond to an altitude maximum of 300m.

The wind simulation model results in turbulence intensity levels of 7.2m/s (3σ), for wind speeds of 10m/s. This simulation result agrees with the Medium altitude definition of turbulence intensities associated with Moderate wind conditions quoted in the NATO report [0].

Gust lengths and amplitudes of 120m and 3.5m/s respectively were chosen to reflect conditions at low altitudes. Horizontal gusts only were considered for this study, because of the proximity to ground.

The XRAE test harness was used to examine the robustness of the modified autopilots using the wind models and the speed, height and yaw test harness step demands described in the previous sub-sections. The controllability of the airframe is limited by the stall incidence, which occurs when the incidence exceeds 11°, and by the maximum fin deflections of:

$$|\xi|_{\max} = 18^\circ, \; |\eta|_{\max} = 14^\circ, \; |\varsigma|_{\max} = 13.6^\circ$$

Since the lift data is only available down to -5°, and to allow a reasonable contingency to avoid stall, the acceptable incidence region was chosen to be limited to $-5^\circ < \alpha < 5^\circ$. For negative incidences $(\alpha < -5^\circ)$ the lift coefficient is extrapolated in the CCS 6DOF model.

Using this test harness including the modified adaptive autopilots, robustness, in the sense of not exceeding the fin and incidence limits, was achieved for turbulence associated with wind speeds of less than 5m/s.

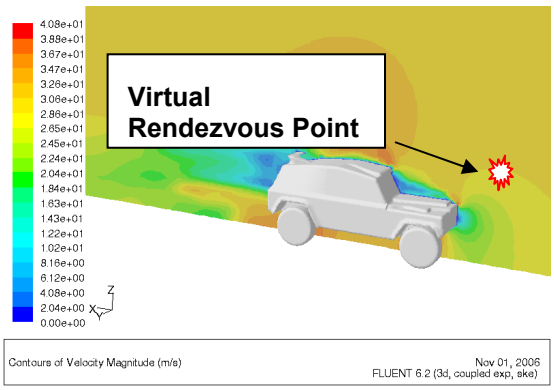

Figure 6: UGV Turbulence prediction

Intimate Control Performance using Virtual Rendezvous Point

To avoid the worse areas of the UGV flowfield, see Figure 6, the rendezvous guidance scheme was reformulated to force the UAV to approach the UGV from the front aspect, using a virtual rendezvous point displaced by 10m along the UGV's x-axis. A typical rendezvous, achieved using

this virtual rendezvous point, is shown in Figure 7 with the simulated wind and road roughness disturbances shown in Figure 8.

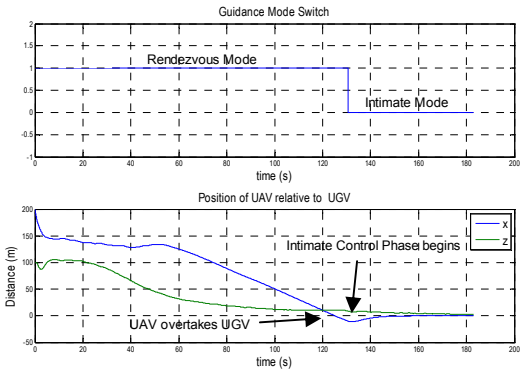

Figure 7: Virtual rendezvous disturbances

The CCS 6FOF model, including the sensor and communications characteristics, described earlier was used to produce a Monte Carlo simulation of this intimate control algorithm. This simulation revealed a reduction in the wind disturbance rejection capability, with wind speeds having to be kept below 3m/s to achieve docking position errors of less than 0.3m, see Figure 8.

Preliminary Autopilot Re-Design: Overcoming Autopilot Sensitivity to Wind Disturbance

To make use of XRAE's gust insensitive configuration the original pitch autopilot was re-designed using the following loop shaping approach [0,0] and tested in a linear pitch test harness.

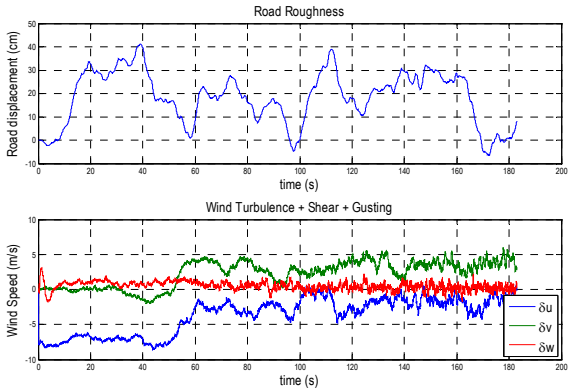

Figure 8: Performance using Virtual Rendezvous Point

The pitch plant for the XRAE vehicle is given by the following state space description:

$$\left\{\begin{array}{l}\begin{bmatrix}\dot{w}\\ \dot{q}\end{bmatrix} = A\begin{bmatrix}w\\ q\end{bmatrix} + B\eta, \quad w = C\begin{bmatrix}w\\ q\end{bmatrix}\\ A = \begin{bmatrix}z_w & z_q + V_m\\ m_w & m_q\end{bmatrix}, B = \begin{bmatrix}z_\eta\\ m_\eta\end{bmatrix},\\ C = \begin{bmatrix}1 & 0\end{bmatrix}, D = 0,\end{array}\right.$$

$$\Rightarrow P(s) = C(sI - A)^{-1}B$$

where s is the Laplace operator, w and q are the pitch linear and angular velocities, V_m is the UAV speed, and $[z_w, m_w, m_q, z_\eta, m_\eta]$ are the pitch trim aerodynamic derivatives. The trim derivative $z_q << Vm$ is small, and is therefore neglected in this autopilot design.

Prior to loop shaping and robust stabilisation, the 2nd order actuator representation is appended to the pitch state space model $P(s)$, to take account of the phase loss produced by this actuator.

Initially the required bandwidth necessary to reject wind disturbances was established using the SIMULINK environment blocks for the wind Turbulence, Shear and Gust disturbances as described earlier. To reject wind disturbances associated with wind speeds up 15m/s and gust up to 3m/s, the required autopilot bandwidth was found to be ~25rad/s.

The Matlab function NCFSYN was then used in this loop shaping process to compute an H_∞ optimal controller which minimises the following cost function,

$$\gamma_{\min} = 1/\varepsilon_{\max} = \min_{\text{stabilising K}} \left\| \begin{matrix} S & T \\ KS & KT \end{matrix} \right\|_\infty$$

where the sensitivity S and complementary T sensitivity functions are given by:

$$S = (I + G)^{-1}, \quad T = (I + G)^{-1} G$$

To achieve the required disturbance rejection bandwidth of 25rad/s, the following loop shaping gain:

$$W_v = \frac{s+5}{2s}$$

was used to shape the inner velocity loop:

$$\mathrm{G} = \mathrm{Act} * \mathrm{P} * \mathrm{W_v} * \mathrm{K_v}$$

where $\mathrm{K_v}$ is the resulting H_∞ stabilising inner loop velocity controller. This loop shaping gain was also chosen to keep the gain roll off close to 20dB/decade in order to produce a control solution with an optimal phase margin. The resulting singular value plot of the H_∞ controlled inner velocity loop is shown in Figure 9.

Finally, with the velocity loop closed using the velocity compensator $\mathrm{W_v} * \mathrm{K_v}$, the same loop shaping procedure was applied to the height loop where the height plant to be stabilised is given by

$$-G(1+G)^{-1}\left(\frac{1}{s}\right)$$

The loop shaping gain used to ensure that the height loop gain rolls off at approximately 20dB/decade at the 0dB cross over point was chosen to be:

$$W_h = \frac{s+0.001}{2s}$$

The singular value plot of this height loop, including the stabilising and loop gain shaping controllers $\mathrm{K_h}$, $\mathrm{W_h}$, given by:

$$\mathrm{G_v} * (\mathrm{G}+1)^{-1} \frac{1}{s} \mathrm{W_h} * \mathrm{K_h}$$

is shown in Figure 9, with a roll off of ~ 25dB/decade at the cross over frequency of 0.5rad/s.

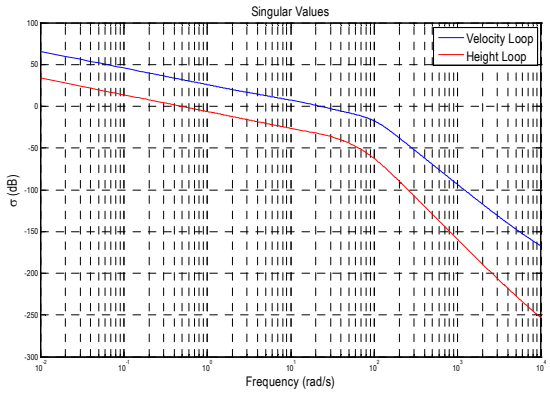

Figure 9: Pitch Autopilot Open Loop Frequency Response

The step responses of the inner velocity and outer height loops are shown in Figure 10.

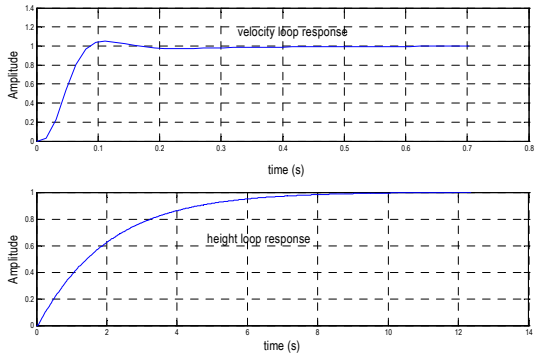

Figure 10: Pitch loop shaping controller Step response

The improved wind disturbance suppression achieved using this loop shaped pitch autopilot with its higher inner loop bandwidth is shown in Figure 11. The first plot in this figure shows the perturbation in pitch velocity δw due to turbulence and shear, with gusting occurring at 40s. The second plot shows that in response to these disturbances the fin positions and rates remain within their limits. And the third plot shows that with the exception of the unlikely vertical gust disturbance, the resulting pitch displacement is less than 0.2m.

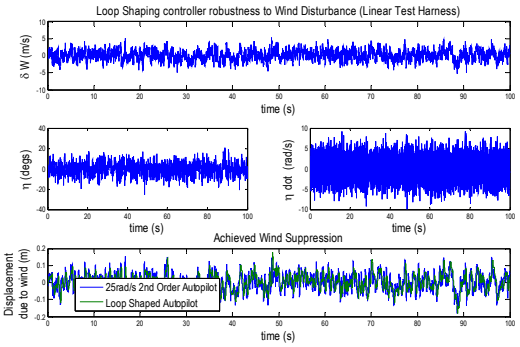

Figure 11: Pitch loop shaping controller Wind Disturbance Rejection

Sensors and Communications

To implement this intimate control strategy, see [0], the UAV would require: a measurement of air and ground speed; a 3-axis gyro and accelerometer; an altimeter to avoid the ground and allow the UAV to approach the UGV at a favourable height to minimise the disturbance due to the UGV's flowfield; and a GPS receiver.

Similarly the UGV would require: a 3-axis gyro and accelerometer pack; and a GPS receiver.

During the Rendezvous Guidance phase, UGV position, velocity and attitude would need to be communicated to the UAV. Assuming single bit precision (32 bits), the Rendezvous Guidance communication bandwidth should accommodate a bit rate of $9.6kbs^{-1}$ [0]. During the Intimate Control phase the UGV position, velocity, acceleration and attitude vectors together with the speed and latax demands would need to be transmitted between the UGV and UAV resulting in a bit rate requirement of $0.48Mbs^{-1}$ [0].

Conclusions

With the current XRAE airframe modified to include an airbrake, which increases the drag by 50%, together with the modified autopilots, which take into account the phase loss from the actuators, rendezvous can only be guaranteed for wind speeds less than 3m/s.

If the XRAE airframe were selected for a demonstration of intimate control, the autopilots would need to be completely re-designed to improve stability and to decrease the UAV's sensitivity to wind disturbances. The preliminary loop shaped H_∞ pitch autopilot design, obtained using a linear representation of the pitch aerodynamics, showed that wind disturbances can be tolerated for wind speeds up to 15m/s using the XRAE airframe.

References

[1] Griffiths, T., (2007), *Collaborative Control Phase 2: Stage1 – Preliminary Analysis*, Unpublished SEAS DTC report

[2] Griffiths, T., (2007), *Collaborative Control Phase 2: Stage1 – Communications and Sensors Requirements*, Unpublished SEAS DTC report.

[3] Gate. Martin, *Collaborative Control Phase 1*, Unpublished SEAS DTC report.

[4] Karagiannis, Dimitrios, *Modelling and Simulation of the XRAE Aircraft*, Dept. Electrical and Electronic Engineering, Imperial College London, February 2005

[5] Gillespie, T.(1992), *Fundamental of Vehicle Dynamics*, Society of Automotive Engineers (SAE), Inc.

[6] Morosiuk,G., Jones, C., Osman, M., *Calibration and standardisation of road roughness measurements using TRL beam*, Transport Research Laboratory, Proceedings of the Seventh REAAA Conference, Singapore, June 1992.

[7] Futaba Servo Motors, www.active-robots.com

[8] U.S. Military Specification MIL-F-8785C, 5 November 1980

[9] *Collaboration for Land, Air, Sea and Space Vehicles: Developing the Common Ground in Vehicle Dynamics, System Identification, Control, and Handling Qualities*, NATO RTO Technical Report 61, November 2002

[10] McFarlane, D.C., and K. Glover, *Robust Controller Design using Normalised Coprime Factor Plant Descriptions*, Springer Verlag, Lecture Notes in Control and Information Sciences, vol. 138, 1989.

[11] McFarlane, D.C., and K. Glover, *A Loop Shaping Design Procedure using Synthesis*, IEEE Transactions on Automatic Control, vol. 37, no. 6, pp. 759-769, June 1992.

Acknowledgements

The work reported in this paper was funded by the Systems Engineering for Autonomous Systems (SEAS) Defence Technology Centre established by the UK Ministry of Defence.